Enhancement of skyrmion density via interface engineering

Sabpreet Bhatti, H. Tan, M. Sim, V. Zhang, M. Sall, Z. Xing, R. Juge, R. Mahendiran, A. Soumyanarayanan, S. Lim, et al.

APL Materials

RESEARCH ARTICLE | JANUARY 13 2023

Enhancement of skyrmion density via interface engineering

Sabpreet Bhatti ; H. K. Tan ; M. I. Sim ; V. L. Zhang ; M. Sall; Z. X. Xing; R. Juge ;
R. Mahendiran ; A. Soumyanarayanan ; S. T. Lim ; D. Ravelosona ;
S. N. Piramanayagam

APL Mater. 11, 011103 (2023)
https://doi.org/10.1063/5.0118147

Enhancement of skyrmion density via interface engineering

Cite as: APL Mater. 11, 011103 (2023); doi: 10.1063/5.0118147
Submitted: 3 August 2022 • Accepted: 16 December 2022 •
Published Online: 13 January 2023

Sabpreet Bhatti,[1] H. K. Tan,[2] M. I. Sim,[2,3] V. L. Zhang,[4] M. Sall,[5] Z. X. Xing,[2] R. Juge,[5] R. Mahendiran,[3] A. Soumyanarayanan,[2,3,a)] S. T. Lim,[2,a)] D. Ravelosona,[5,6,a)] and S. N. Piramanayagam[1,a)]

AFFILIATIONS

[1] School of Physical and Mathematical Sciences, Nanyang Technological University, Singapore
[2] Institute of Materials Research and Engineering, Agency for Science, Technology and Research A*STAR, Singapore
[3] Department of Physics, National University of Singapore, Singapore
[4] Wuhan University, Hubei, China
[5] Spin-Ion Technologies, 10 Boulevard Thomas Gobert, 91120 Palaiseau, France
[6] Centre de Nanosciences et de Nanotechnologies, CNRS, Université Paris-Saclay, 10 Boulevard Thomas Gobert, 91120 Palaiseau, France

[a)] **Authors to whom correspondence should be addressed:** anjan@nus.edu.sg; Lim_Sze_Ter@imre.a-star.edu.sg; dafine.ravelosona@c2n.upsaclay.fr; and prem@ntu.edu.sg

ABSTRACT

Magnetic skyrmions are promising candidates for computing and memory applications. The static and dynamic behaviors of skyrmions are tunable by altering the interfacial magnetic properties. These interfacial magnetic properties are alterable by modifying the interface structure of thin films. However, the relationship between the structural properties of the interface and the skyrmions properties is not straightforward, and a comprehensive insight is required to facilitate better controllability of the skyrmions' behaviors. Here, we comprehensively understand the relationship between atomic displacements at the interface and skyrmions' static behavior. In this study, we used ion irradiation to achieve inter-atomic displacements. We observed that the inter-atomic displacements could tailor the physical properties of skyrmions. We noticed a peculiar increase in the magnetization, Dzyaloshinskii–Moriya interaction, and exchange stiffness. The modifications in magnetic properties reduced the domain wall energy, which enhanced the skyrmion density (by six-folds) and reduced the average skyrmion diameter (by 50%). Furthermore, we compared the observed results of ion irradiation with those from the annealing process (a well-studied method for modifying magnetic properties) to better understand the effect of atomic displacements. Our study provides a route to achieve a highly-dense skyrmion state, and it can be explored further to suppress the skyrmion Hall effect for skyrmion-based applications.

INTRODUCTION

Skyrmions are chiral spin textures that have gained considerable interest due to their promising applications in memory and computing.[1–3] In a specific material system, skyrmion's behavior is affected by magnetic properties. Dzyaloshinskii–Moriya interaction (DMI), an anti-symmetric exchange interaction induced by spin–orbit coupling, is a crucial property for the existence and stability of skyrmions in thin films.[4–6] A relative change in the DMI as compared to the effective magnetic anisotropy (K_{eff}) and exchange stiffness constant (A_{ex}) can impact the density, size, and thermal stability of skyrmions.[7–13] Such changes in magnetic properties were achieved through approaches like variation in the stoichiometry and thickness of the ferromagnetic (FM) layer.[9,14,15] The approaches were able to control the skyrmions' physical properties up to some extent.

Ion irradiation is a useful technique that induces displacement and recombination of atoms in a target sample. The irradiation

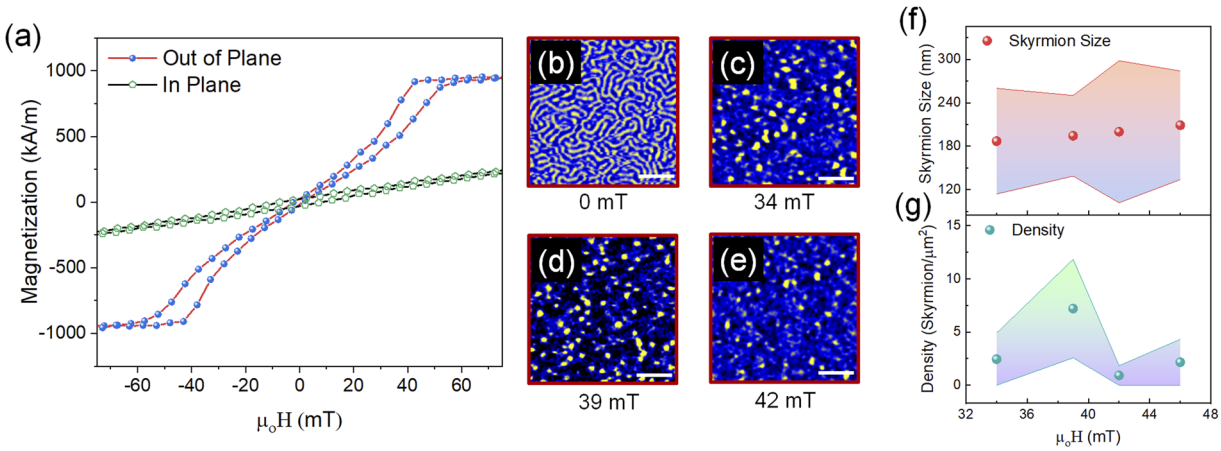

FIG. 1. Field-dependent skyrmion properties of the pristine sample. (a) MH loops of the pristine sample. (b)–(e) MFM images of magnetic textures observed at various fields (applied in out-of-plane direction). The scale bar represents 1 μm length. (f) and (g) are the plots of skyrmion size. The pristine sample shows a maximum density at a field of 39 mT. [Shades in (f) and (g) represent the spread in measured values, achieved by fitting all skyrmions accepted after the filtering process.]

of light elements like Helium follows a simple ballistic recoil mechanism model.[16–21] He^+ ions irradiation in an energy range of 10–30 keV induces short-range atomic displacements (in the order of a few inter-atomic distances) without causing harsh material damage like surface sputtering or cascade collisions.[22] Moreover, for doses lower than 10^{20} ions/m^2, the roughness of the interface can remain almost unaffected, and the morphology of the layers does not show any blistering effect.[18,23] The structural modifications induced by ion irradiation alter the magnetic properties of material systems.[24,25] As shown recently, ion irradiation can induce the nucleation of magnetic skyrmions.[26,27] However, these studies failed to achieve the required change in magnetic properties. Moreover, in these studies, the complex interplay between the changes in structural properties and the resulting skyrmion nucleation was not clearly established.

In this article, we comprehensively understand the effect of interfacial atomic displacements on the physical attributes of skyrmions. We have used He^+ irradiation to induce the displacement of atoms at the interface of thin films and lateral displacements of atoms within the FM layer. The atomic displacements resulted in an enhancement of the magnetostatic energy, which substantially influenced the bulk (exchange energy and saturation magnetization) and interfacial (surface anisotropy and DMI) magnetic properties. The changes in magnetic properties enhanced the skyrmion density by six-folds while reducing the skyrmion diameter by 50%. We performed various structural analyses to understand the effect of irradiation on the structure of thin films, which affected skyrmion properties. Furthermore, we have annealed our samples, a well-studied method for modifying magnetic properties, to compare and understand the effect of atomic displacements on magnetic properties. Our study provides a comprehensive understanding of the effect of interfacial atomic displacements on the attributes of skyrmions.

We performed this study on a multilayer stack consisting of $[Pt(3)/Co_{60}Fe_{20}B_{20}(0.5)/MgO(1.5)]_8$ (thickness in nanometer), which was deposited on a SiO_x wafer (see the "Experimental Section"). After deposition, we did not anneal the sample (hereafter referred to as pristine sample), which kept the FM layer in an amorphous state.[28–30] We irradiated the pristine sample with a He^+ ion beam at different doses (ion fluences), varying from 0 to 12 $\times$ 10^{18} ions/m^2 (10^{14} ions/cm^2)[31] (see the "Experimental Section"). We investigated the changes in structural properties using time-of-flight secondary ion mass spectroscopy (ToF-SIMS), cross-sectional energy-dispersive x-ray spectroscopy (EDS), and Monte Carlo simulations. We probed the magnetic properties by employing a vibrating sample magnetometer (VSM) and an alternating gradient field magnetometer (AGM). In addition, we measured the DMI using Brillouin light scattering (BLS) spectroscopy.[32,33] For estimating A_{ex}, we used micromagnetic simulations. We used a magnetic force microscope (MFM) to examine the size and density of skyrmions.

We started by examining the pristine sample. The sample exhibits a perpendicular magnetic anisotropy with a K_{eff} of 140 kJ/m^3. The magnetic hysteresis (MH) loop of the sample shows a shear trait [Fig. 1(a)]. The MFM imaging at zero field revealed a labyrinthine magnetic texture with a nearly equal area of up and down magnetized domains [Fig. 1(b)]. When imaged at external magnetic fields ($\mu_0 H$), the stripe domains transformed into skyrmions [shown in Figs. 1(c)–1(e)]. The observation of skyrmions in the pristine sample implies the existence of a sizable interfacial DMI required for their room temperature stabilization.[34] Field-dependent imaging revealed the highest skyrmion density of 7.2 skyrmion/μm^2 at 39 mT [Fig. 1(f)]. The average size of skyrmion varied over 100–250 nm [Fig. 1(g)] under different external fields. This variation infers a relatively large distribution of skyrmion size.

MODULATION OF STRUCTURAL PROPERTIES

We began the investigation of irradiated samples by ToF-SIMS. The relative intensities and positions of ToF-SIMS peaks for irradiated and pristine samples can infer the displaced atoms.[35–37] We compared the peak intensities of 8× and 12× samples with the

pristine sample (hereafter, n being an integer n× representing the multiple of 10^{18} ions/m^2 for dose and 10^{14} ions/cm^2 for ion fluence). The observation of eight repetitive peaks (after irradiation) for all elements of layers (see the supplementary material) validated the intactness of the layers after irradiation. We normalized the intensity of the peak by dividing it with an area under the curve of the pristine sample peak (the first peak of the same element). The 8× sample lacked any significant reduction in the Co, Fe, and B intensities [Figs. 2(a)–2(c)]. In addition, the intensity [Fig. 2(d)] and the position of the Mg peak for the 8× sample were unchanged, eliminating any possibility of Mg intermixing into the FM layer [Figs. 2(d) and 2(e)]. We speculate that the lack of noticeable changes for the 8× sample may be due to the limited resolution of the ToF-SIMS measurement.

On the contrary, for the 12× sample, the Co and Fe intensities were reduced [Figs. 2(a) and 2(b)], which may arise from the displacement of atoms.[36] The reduction was observed for all peaks of the 12× sample (see the supplementary material). We did not notice any significant broadening in the peaks of FM atoms. Interestingly, we noticed a slight reduction in the intensity of B. The reduced intensities of FM atoms (unlike the 8× sample) resulted from the increased He^+ bombardments, suggesting the displacement of the FM atoms. Although we did not observe any reduction in the intensity of the Mg peak [Fig. 2(d)], we noticed a shift in the peak position [Fig. 2(e)]. We speculate that the shift in peak is due to the shifting of Mg atoms from the Mg layer to the FM layer.

The unchanged intensity of B peaks of 8× and similar intensity of 12× samples [Fig. 2(c)] questions the sensitivity of the used ToF-SIMS instrument against B. We answered this question by characterizing an annealed (300 °C) unirradiated sample. Annealing of the CoFeB layer induces the migration of B atoms, leading to its crystallization.[39,40] We observed a reduced peak intensity of B after annealing (see the supplementary material), which signifies the suitability of used ToF-SIMS equipment for detecting B. Noticeably, the B peaks of pristine and irradiated samples showed an asymmetric nature, which reflects the asymmetric diffusion of B in the FM layer. In addition, we noticed a slight shift in the asymmetry of peaks toward the MgO/CoFeB interface with an increase in the irradiation dose. We speculate that the ion irradiation may induce heating to the samples, and as reported, B migration can occur in a few seconds due to the heating,[41,42] which might have resulted in formation of a MgBxOy layer at the interface.[43]

Next, we visualized the effect of ion irradiation on the 8× sample structure via EDS. We observed that the Co layers remained at their positions, corroborating the ToF-SIMS results [Figs. 2(f) and 2(g)]. Notably, we saw the displacement of Co atoms at the CoFeB/Pt interface [Fig. 2(g)] and roughening of the Co layer at MgO/CoFeB interface. The displaced Co atoms at CoFeB/Pt interface infer the intermixing of Co and Pt atoms. In contrast to Co layers, Pt layers were still intact and lacked any considerable movement of atoms [Figs. 2(h) and 2(i)] between two adjacent Pt layers. Unlike ToF-SIMS, EDS results showed the displacement of atoms in the 8× sample. However, ToF-SIMS indicated the displacement of atoms in the 12× sample only. This implies that the changes in the 12× sample were significant to get detected by ToF-SIMS. Hence, we concluded that the displacement of atoms was increased with an increase in the irradiation dose. Moreover, the EDS results of 8× showed a minute broadening of the Mg layer and did not depict any displacement of Mg atoms (similar to the ToF-SIMS results for 8× Mg).

Interestingly, sputter deposition of MgO on the CoFeB layer can result in the oxidation of FM atoms.[43,44] While ion

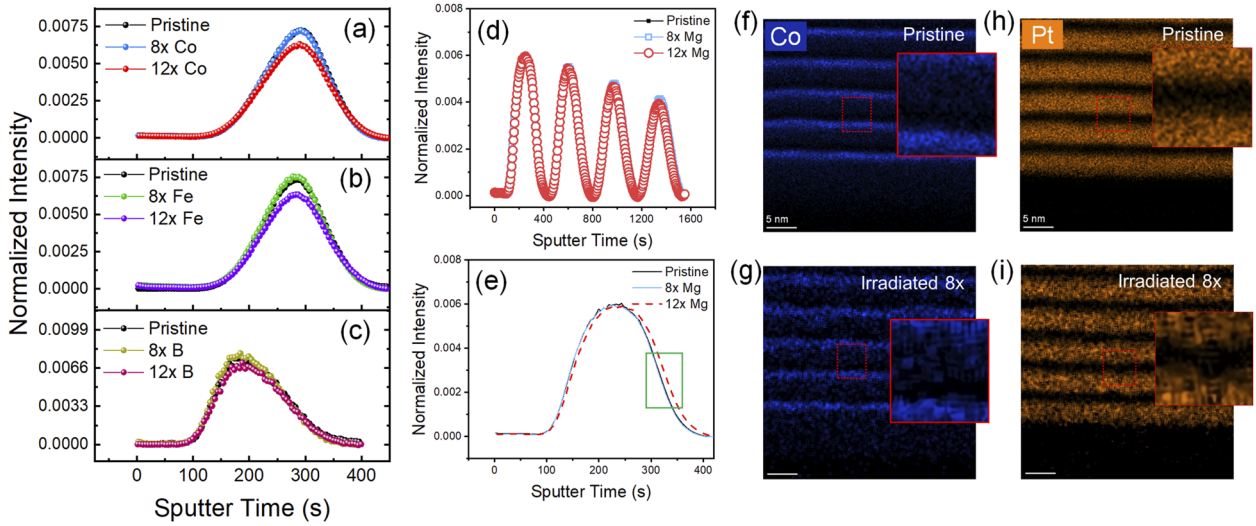

FIG. 2. Modulation in the structural properties due to different ion doses (fluences). (a)–(c) ToF-SIMS intensities of Co, Fe, and B for the pristine, 8×, and 12× samples for the top layer. The intensities were normalized with respect to the area under the curve of peaks from the pristine sample. (d) ToF-SIMS intensities of Mg for the pristine, 8×, and 12× samples. The decrease in the amplitude of peaks with respect to the sputtering time is due to reduced sputter yield during the sputtering process of ToF-SIMS.[38] (e) The zoomed-in first peak of Mg for the pristine, 8×, and 12× samples. The shift in the position of the 12× peak is highlighted (the green box). (f) and (g) Cross-sectional EDS of Co for pristine and irradiated 8× samples (shown by zoomed-in region). (h) and (i) Cross-sectional EDS of Pt for pristine and irradiated 8× samples.

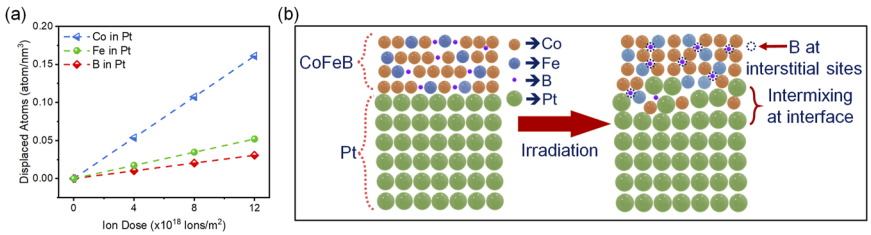

FIG. 3. Predicted displacements of atoms due to He^+ ion irradiation. Monte Carlo simulations (TRIM) on the displacement of atoms. (a) Plot for ferromagnetic atoms migration into the Pt layer. Intermixing of ferromagnetic atoms increases linearly with the ion dose. (b) Schematics of irradiation induced displacements depicting intermixing at interface and B substituting at interstitial sites.

irradiation-driven intermixing can, in principle, induce such oxidation, this is expected to reduce the resulting magnetization. The increased magnetization observed upon irradiation for our samples (discussed in the next section) indicates that such oxidation, even if present, is unlikely to play an important role in our work.

We further investigated the effect of ion irradiation on the structure of pristine samples via Monte Carlo simulations[45–47] (see the supplementary material). The simulations suggested the displacement of FM atoms (Co, Fe, and B) into the Pt layer and intermixing of atoms at the interface of the CoFeB and Pt layers [Fig. 3(a)]. The higher number of displaced Co atoms (predicted per cubic nm) than that of Fe and B atoms is a result of the higher stoichiometry of Co in the FM layer. The atomic displacements were increased with the irradiation dose,[48] corroborating the ToF-SIMS results. Moreover, the simulations predicted the lateral displacements of FM atoms inside the FM layer, which were higher than those in the Pt layer (see the supplementary material). Since the FM layer is amorphous, Co and Fe atoms can swap with each other, resulting in a negligible effect on the structure and magnetic properties. In contrast, the lateral displacement of B can result in B substituting between Co and Fe atoms [Fig. 3(b)], which may affect the properties.[42,49,50]

MODIFIED MAGNETIC PROPERTIES

We measured magnetization curves to probe the effect of atomic displacements on magnetic properties. We noticed an increase in the saturation field ($\mu_0 H_s$) of MH loops [Fig. 4(a)]. In addition, the loops became narrower (losing their sheared trait) with increased irradiation dose (see the supplementary material). Moreover, we found that the M_s was increased, reaching 150% for 8× dose [Fig. 4(b)]. We reconfirmed the enhanced M_s by measuring the MH loops by an AGM. Furthermore, we quantified the increase in $\mu_0 H_s$ [Fig. 4(c)] using first order reversal curves[51] (see the supplementary material). We further noticed that K_{eff} decreased monotonically when the irradiation doses increased [Fig. 4(c)].

The increase in M_s [Fig. 4(b)] might arise due to intermixing of FM and Pt atoms at the interface and migration of B. The intermixing of Co (Fe) with Pt results in the formation of magnetic CoPt (FePt) alloy, which may further increase magnetic moment due to band narrowing and reduction of nearest neighbors.[52] Additionally, the immediate proximity of Co with Pt can induce magnetic moment to Pt atoms,[53–56] thereby decreasing the effective thickness of the dead layer (0.2 nm for the pristine sample) while increasing the total magnetic moment. The reduction in the dead layer, along with the possible migration of B (discussed in the ToF-SIMS section), can increase M_s by 35%.[57] We separately examined the possible increase in M_s by annealing the pristine sample at various temperatures. The annealed samples resulted in an enhanced M_s, where the M_s was increased up to a similar value of 8× sample (see the supplementary material). This outcome supports that the two effects can cause the enhancement of M_s. Meanwhile, the reduced M_s of the highest dose sample (12×) can be explained due to the shifting of non-magnetic element (Mg) into the FM layer and high intermixing of Co and

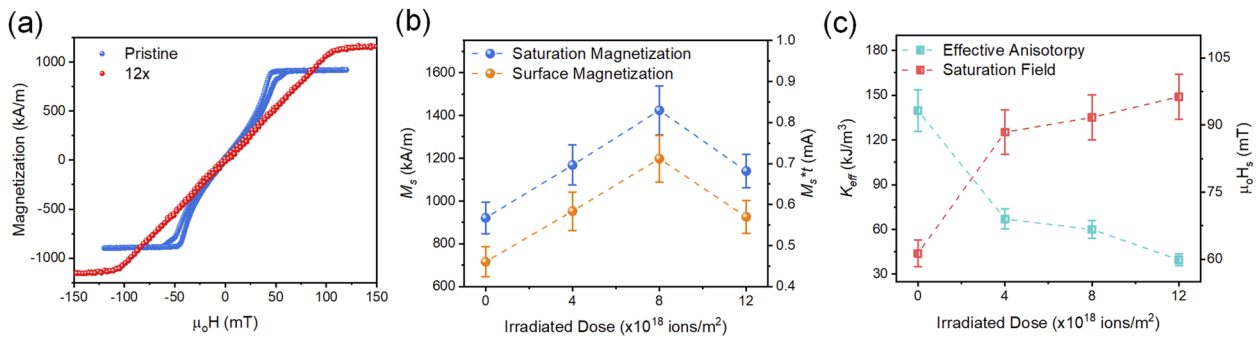

FIG. 4. Magnetic properties of irradiated samples. (a) MH loops of pristine and 12× sample. M_s increased after irradiation. (b) Variation of saturation magnetization M_s and surface magnetization $M_s \times t$ with varying irradiation doses (fluences). (c) Effective magnetic anisotropy energy density and saturation field (out of plane) for different ion doses.

Pt atoms,[58,59] which reduces the magnetization. Previous studies on He^+ irradiation of CoFeB material systems did not show enhanced M_s. The lack of such behavior can be explained due to the use of annealed material systems in the previous studies.[22,36,60,61] The annealed system had already gone through B migration during the annealing and, hence, did not show any increase in M_s after irradiation. Moreover, we eliminated any possible discrepancy in the effective thickness of the FM layer by calculating surface saturation magnetization ($M_s \times t$) [Fig. 4(b)]. The reduced K_{eff} with increase of interfacial atomic displacements is a direct repercussion of disordering at the interface between FM and Pt layers,[62,63] observed in the structural characterizations. In contrast, the increased $\mu_o H_s$ and narrowness in the MH loops after irradiation are the outcome of weaker perpendicular magnetic anisotropy and enhanced magnetostatic energy.[28,30,64] In addition, we saw that the uniaxial anisotropy (K_u) was increased after irradiation even when the K_{eff} was reduced (see the supplementary material). We concluded that the increased K_u is an attribute of the enhanced magnetostatic energy.

Next, we measured the DMI of samples using BLS.[32,33] The DMI induces an asymmetry of the magnon dispersion, which leads to the difference in the frequencies of Stokes and Anti-Stokes peaks (Δf). We noticed that Δf [shown in Fig. 5(a) for the pristine sample] stayed constant up to 8× dose and reduced by 15% for 12× dose (see the supplementary material). When calculated, the magnitude of the DMI followed the trend of M_s [Fig. 5(b)]. Furthermore, we replaced M_s with surface magnetization ($M_s \times t$) to

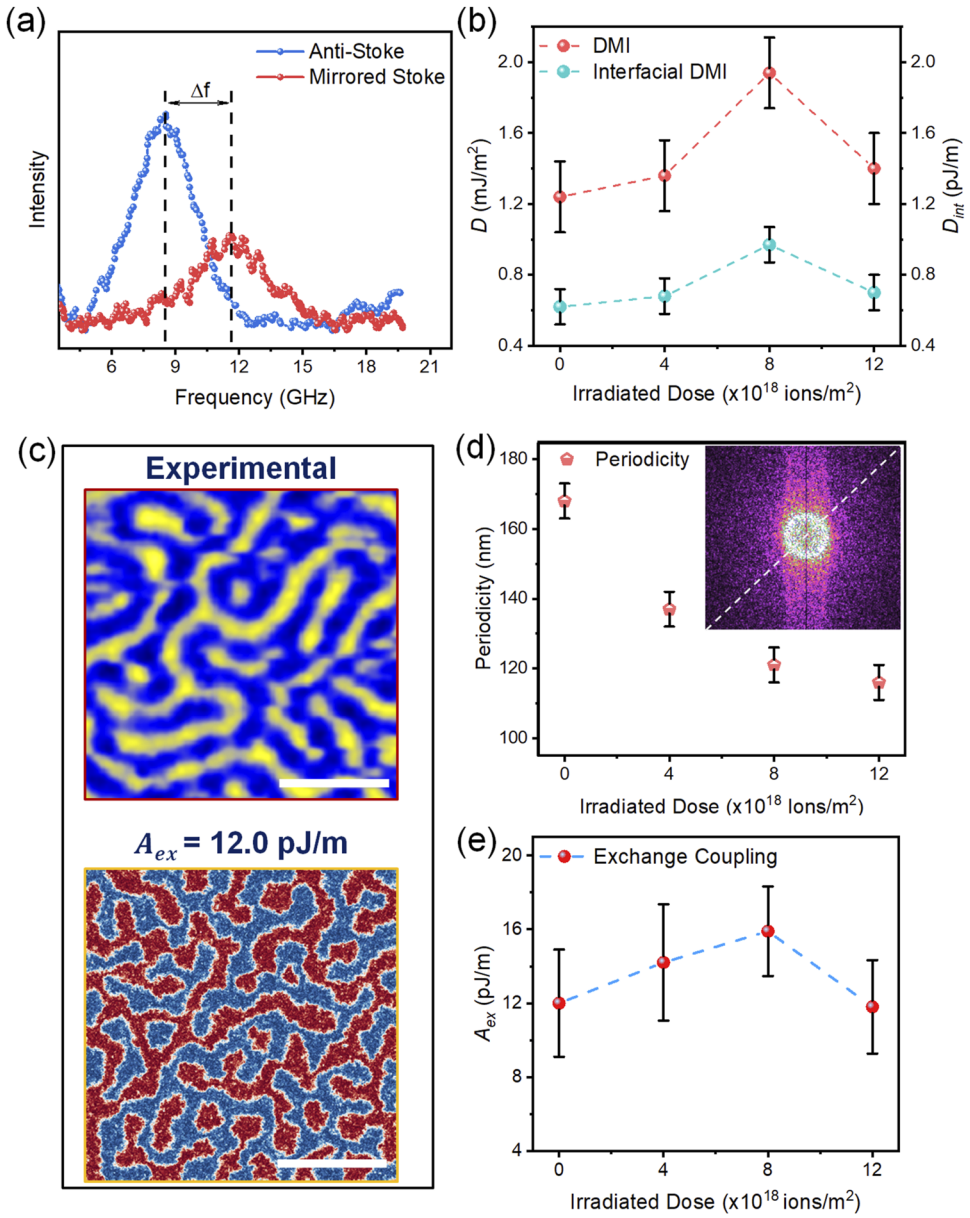

FIG. 5. Determination of exchange interactions. (a) BLS spectra of the pristine sample measured at k_{sw} = 16.7 μm^{-1}, mirrored around Δf = 3.1 GHz for clarity of presentation. (b) Variation of effective micromagnetic DMI (D) and interface DMI (D_{int}) as a function of irradiated dose. (c) Experimental MFM image of the pristine sample (top) and simulated magnetic textures with the same periodicity of MFM image, achieved at 12 pJ/m (bottom). The scale bar represents 500 nm length. (d) Effect of irradiation dose on the periodicity of experimental magnetic textures observed at zero field. The inset shows the 2-D FFT profile of zero-field magnetic textures of the pristine sample. (e) Estimated A_{ex} values for different ion doses (fluences).

eliminate any discrepancy in the effective thickness of the FM layer and calculated the interfacial DMI (D_{int}) [Fig. 5(b)].[48,52] The calculated DMI value of the pristine sample (1.25 mJ/m^2) agrees well with those of previous studies.[65–67] For the irradiated samples, we found an increase in DMI, which was the maximum for 8× sample (1.94 mJ/m^2). As reported previously, the interface intermixing between FM and heavy metal atoms at a rough interface may increase D and D_{int} by a few percent.[48,52,68,69] Here, the enhanced DMI by 50% (and the trend of DMI) is a peculiar feature of our study. Intermixing of Co and Pt layers can increase the formation of Co–Pt–Co triplets, thereby introducing additional asymmetric exchange interactions and, hence, resulting in an enhancement in the DMI. Additionally, we speculate that the enhanced magnetostatic energy might have contributed to the increase in the DMI. On the contrary, for the higher dose sample (12×), the drop in DMI is due to large disordering at the CoFeB/Pt interface.[52]

We estimated the A_{ex} using a combination of micromagnetic simulations (Mumax3[70]) and experiments (see "Experimental Section"). In simulations, we varied the value of A_{ex} (keeping other parameters constant) and achieved equilibrium states (at zero field) with various periodicities.[9,66,71,72] We compared the periodicities of simulated states[9,73] (see the supplementary material) with the extracted periodicity values from the MFM images [Fig. 5(d)] to achieve A_{ex} [Fig. 5(c)]. Interestingly, the estimated A_{ex} for irradiation samples [Fig. 5(e)] follows the trend of M_s, revealing the dependence of A_{ex} on the magnetostatic energy.[74] We speculate that the variation of A_{ex} after irradiation is due to the changes in the structure of the FM layer, which also led to the trend of M_s.

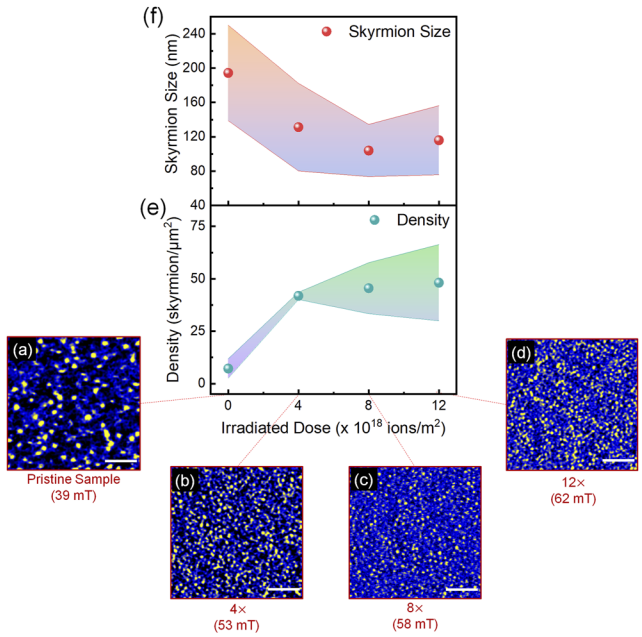

FIG. 6. Effect of interface intermixing on the physical properties of skyrmions. (a)–(d) MFM images of pristine, 4×, 8×, and 12×, respectively. Images were captured at the out-of-plane magnetic fields corresponding to the maximum skyrmion density. (e) Variation in skyrmion density due to different ion doses (fluences). (f) Average skyrmion size at different ion doses (fluences).

EVOLUTION OF SKYRMION PHYSICAL PROPERTIES

We imaged the irradiated samples at different magnetic fields. Figures. 6(a)–6(d) show MFM images of samples at their highest skyrmion density states. We noticed an increase in the skyrmion density of irradiated samples. The increase in the density was more than six-fold, increasing up to 48.12 skyrmion/μm^2 [Fig. 5(e)]. In addition, we quantified the skyrmion size at the fields where skyrmion densities were the highest. We found a reduction in the variance of skyrmion size by almost 50%, where the size of the smallest skyrmion reduced from 139 to 76 nm [Fig. 5(f)]. Moreover, we measured the average skyrmion eccentricity and found that the skyrmions became more circular with increased irradiation dose. However, the change was not as significant (see the supplementary material) as reported in a previous study.[27]

The increase in the density of zero-field magnetic textures [Fig. 5(d)] and skyrmions [Fig. 6(e)] is due to the following factors: (i) a reduction in K_{eff}, resulting from the modulation of anisotropy and dipolar interactions and (ii) an increase in DMI.[75,76] The modification of these magnetic properties, caused by atomic displacements, resulting in a lower domain wall energy[8] (see the supplementary material). The combination of these two factors favors the formation of densely packed skyrmions.[9]

SUMMARY AND OUTLOOK

Atomic displacements provide a route to tune the interfacial and bulk magnetic properties of chiral magnetic material. The alloying of Co (Fe) and Pt atoms, increase in immidiate proximity of Co with Pt, and migration of B atoms led to the enhancement of magnetostatic energy, which, in turn, influenced the DMI and A_{ex}. The disordering at the interface modified both K_{eff} and DMI. The investigations on the stack interface explained the underlying phenomena for variation in the magnetic properties. Consequently, the changes in the magnetic properties led to a reduced domain wall energy. The decreased in domain wall energy enabled denser skyrmion states with smaller skyrmion sizes. These results establish a connection between the atomic displacement-induced modifications of structural properties and the resulting characteristics of skyrmions. Our study demonstrates a technique to tailor the physical properties of magnetic skyrmions to achieve dense skyrmion states. Moreover, the used technique can be exploited to suppress the skyrmion Hall effect by creating energy barriers on the edges, as predicted by previous studies.[77,78] Hence, the study offers a promising perspective for developing high-density skyrmion-based racetrack memory and neuromorphic applications. Moreover, the findings of our report addresses a broad topic that is not only limited to the materials with skyrmions but can be extended to any magnetic material system with crucial attributes from the interfacial structures.

EXPERIMENTAL SECTION

The sample used for this study is Ta(5)/[Pt(3)/$Co_{60}Fe_{20}B_{20}$(0.5)/MgO(1.5)]$_{x8}$/Pt(3) (thickness in nanometers). The film stack was sputter-deposited on a thermally oxidized Si wafer using the 300 mm Singulus Timaris tool. The He^+ irradiation was performed using a Helium-S® system from

Spin-Ion Technologies. The irradiation was done at 20 keV by keeping the ion flux constant at around 9×10^{16} ion m^{-2} s^{-1}. The irradiation dose was varied in the 10^{18} ions/m^2 range, which was integrated over an area of 2.72×10^4 m^2. The samples were annealed in a vacuum annealing oven for 1 h at different temperatures. The ramping time to reach the set temperature was kept constant at 30 min, and after annealing, the samples were left in the oven for overnight to cooldown.

Magnetic properties were measured by Lakeshore 8600 series vector vibrating sample magnetometer (VSM) and MicroMag alternative gradient field magnetometer (AGM). We calculated the K_{eff} using the formula:[79–81] $K_{eff} = M_s\left[\int_0^1 H_{op}(m_{op})dm_{op} - \int_0^1 H_{ip}(m_{ip})dm_{ip}\right]$, where H_{op} and H_{ip} are the applied magnetic field, and m_{op} and m_{ip} are the normalized value of magnetization in the out-of-plane and in-plane directions, respectively (see the supplementary material). Brillouin light scattering (BLS) spectroscopy measurements were performed in the 180° backscattering geometry in ps polarization using the 514.5 nm radiation of an argon-ion laser and a six-pass tandem Fabry–Perot interferometer (used in a previous study[32]). We calculated DMI using the formula[14,32,82] $\Delta f = \frac{2\gamma D k_{sw}}{\pi M_s}$ (k_{sw} is spin wave vector and γ is the gyromagnetic ratio).

Imaging of the magnetic states of samples was done by employing a Bruker Dimension Icon atomic force microscope. The images were analyzed in Fourier space to determine the periodicity of textures at zero-field. The position and width of the Fourier transform peak were used to quantify the periodicity of magnetic domains and error bars, respectively. The skyrmion density was measured by filtering out the artifacts from the tip–sample interaction and background noise. To quantify the skyrmion sizes, 2D isotropic Gaussian fits were carried out on the skyrmions within a ~5×5 μm^2, and the full-width at half-maxima (FWHM) was measured.[9,83] The error bars of the skyrmion size represent a true spread in the observed size of multiple skyrmions. The reported sizes are the raw estimates of skyrmion width, lacking any deconvolution to account for the MFM tip size.

The migration of FM atoms was investigated by a time-of-flight secondary ion mass spectroscopy (ToF-SIMS). Analyses were performed using a TOF·SIMS 5–300 instrument (Ion ToF, Germany). A pulsed 30 keV Bi^+ primary ion beam with a target current of 6.8 pA and a field of view of 100×100 μm^2 was used. Analysis was performed in random raster mode with 128×128 pixels (dose density: 1×10^{13} ions per cm^2). A 500 eV Cs sputter beam with a current of 44 nA on an area of 500×500 μm^2 was used for depth profiling. Profiling was carried out in the interlaced mode. Monte Carlo simulations, to predict the effect of irradiation, were carried out by transport of ions in matter (TRIM) software (details of parameters are provided in the supplementary material).

Cross-sectional imaging through a transmission electron microscope was performed at Covalent Metrology, USA.

Micromagnetic simulations were carried out by using Mumax3.[70] The simulations were performed at 300 K, and an effective medium model with eight repetitions was used.[9,66,71,72] The multilayers were modeled with a mesh size of 3×3 nm^2 over a ~1.5×1.5 μm^2 area for comparison with films. The z length was changed to match the effective length, which was calculated using the effective model method. The magnetization was initiated with a random state, which was allowed to run up to 150 ns to achieve an equilibrium state with minimum energy. Finally, the periodicity trends with varying A_{ex} were found to be monotonic, which was used for regression analysis to accurately estimate the magnetic parameters.

SUPPLEMENTARY MATERIAL

See the supplementary material for the supporting data.

ACKNOWLEDGMENTS

The authors would like to thank Dr. Chen Xiaoye, Dr. Pin Ho, Dr. Dickson Thian, and Dr. James Lourembam from the Institute of Materials Research and Engineering, A*STAR Singapore, for the stimulating discussions and valuable suggestions.

This work was supported by the Agency for Science, Technology and Research, A*STAR RIE2020 AME, under Grant No. A18A6b0057.

AUTHOR DECLARATIONS

Conflict of Interest

The authors have no conflicts to disclose.

Author Contributions

Sabpreet Bhatti: Conceptualization (equal); Data curation (lead); Formal analysis (lead); Investigation (lead); Methodology (equal); Project administration (equal); Software (lead); Validation (equal); Visualization (equal); Writing – original draft (lead); Writing – review & editing (equal). **H. K. Tan**: Data curation (supporting); Methodology (supporting). **M. I. Sim**: Data curation (supporting); Formal analysis (supporting). **V. L. Zhang**: Data curation (supporting); Formal analysis (supporting). **M. Sall**: Data curation (supporting). **Z. X. Xing**: Data curation (supporting). **R. Juge**: Formal analysis (supporting); Writing – review & editing (supporting). **R. Mahendiran**: Resources (supporting). **A. Soumyanarayanan**: Conceptualization (equal); Funding acquisition (equal); Methodology (equal); Project administration (equal); Resources (equal); Software (supporting); Supervision (equal); Validation (equal); Visualization (equal); Writing – review & editing (equal). **S. T. Lim**: Conceptualization (equal); Funding acquisition (equal); Methodology (equal); Project administration (equal); Resources (equal); Supervision (equal); Validation (equal); Visualization (equal); Writing – review & editing (equal). **D. Ravelosona**: Conceptualization (equal); Methodology (equal); Resources (supporting); Validation (equal); Visualization (equal); Writing – review & editing (equal). **S. N. Piramanayagam**: Conceptualization (equal); Funding acquisition (equal); Methodology (equal); Project administration (equal); Resources (equal); Supervision (lead); Validation (equal); Visualization (equal); Writing – review & editing (equal).

DATA AVAILABILITY

The data that support the findings of this study are available from the corresponding author upon reasonable request.

REFERENCES

[1] A. Fert, V. Cros, and J. Sampaio, "Skyrmions on the track," Nat. Nanotechnol. **8**(3), 152–156 (2013).
[2] J. Sampaio *et al.*, "Nucleation, stability and current-induced motion of isolated magnetic skyrmions in nanostructures," Nat. Nanotechnol. **8**(11), 839 (2013).
[3] J. Hagemeister, N. Romming, K. Von Bergmann, and E. Y. Vedmedenko, "Stability of single skyrmionic bits," Nature Comm. **6**(1), 1–7 (2015).
[4] A. Fert, "Magnetic and transport properties of metallic multilayers," Mater. Sci. Forum **59**, 439 (1990).
[5] M. Bode *et al.*, "Chiral magnetic order at surfaces driven by inversion asymmetry," Nature **447**(7141), 190–193 (2007).
[6] G. Finocchio *et al.*, "Magnetic skyrmions: From fundamental to applications," J. Phys. D: Appl. Phys. **49**(42), 423001 (2016).
[7] A. Bogdanov and A. Hubert, "Thermodynamically stable magnetic vortex states in magnetic crystals," J. Magn. Magn. Mater. **138**(3), 255–269 (1994).
[8] M. Heide, G. Bihlmayer, and S. Blügel, "Dzyaloshinskii–Moriya interaction accounting for the orientation of magnetic domains in ultrathin films: Fe/W(110)," Phys. Rev. B **78**(14), 140403 (2008).
[9] A. Soumyanarayanan *et al.*, "Tunable room-temperature magnetic skyrmions in Ir/Fe/Co/Pt multilayers," Nat. Mater. **16**(9), 898–904 (2017).
[10] S. Mühlbauer *et al.*, "Skyrmion lattice in a chiral magnet," Science **323**(5916), 915–919 (2009).
[11] X. Z. Yu *et al.*, "Real-space observation of a two-dimensional skyrmion crystal," Nature **465**(7300), 901–904 (2010).
[12] A. O. Leonov *et al.*, "The properties of isolated chiral skyrmions in thin magnetic films," New J. Phys. **18**(6), 065003 (2016).
[13] T. Böttcher *et al.*, "Quantifying symmetric exchange in ultrathin ferromagnetic films with chirality," arXiv:2109.03909 (2021).
[14] J. Cho *et al.*, "Thickness dependence of the interfacial Dzyaloshinskii–Moriya interaction in inversion symmetry broken systems," Nat. Commun. **6**(1), 7635 (2015).
[15] T. Srivastava *et al.*, "Mapping different skyrmion phases in double wedges of Ta/FeCoB/TaOx trilayers," Phys. Rev. B **100**(22), 220401 (2019).
[16] A. Traverse, M. G. L. Boité, and G. Martin, "Quantitative description of mixing with light ions," Europhys. Lett. **8**(7), 633 (1989).
[17] J. F. Ziegler, "The stopping and range of ions in matter," in *Treatise on Heavy-Ion Science* (Springer, Boston, MA, 1985), pp. 93–129.
[18] T. Devolder, "Light ion irradiation of Co/Pt systems: Structural origin of the decrease in magnetic anisotropy," Phys. Rev. B **62**(9), 5794 (2000).
[19] T. Devolder *et al.*, "X-ray absorption analysis of sputter-grown Co/Pt stackings before and after helium irradiation," Eur. Phys. J. B **22**(2), 193–201 (2001).
[20] C. T. Rettner *et al.*, "Characterization of the magnetic modification of Co/Pt multilayer films by He^+, Ar^+, and Ga^+ ion irradiation," Appl. Phys. Lett. **80**(2), 279–281 (2002).
[21] J. Chaumont *et al.*, "A medium energy facility for variable temperature implantation and analysis," Nucl. Instrum. Methods Phys. Res. **189**(1), 193–198 (1981).
[22] X. Zhao *et al.*, "Enhancing domain wall velocity through interface intermixing in W–CoFeB–MgO films with perpendicular anisotropy," Appl. Phys. Lett. **115**(12), 122404 (2019).
[23] F. I. Allen, P. Hosemann, and M. Balooch, "Key mechanistic features of swelling and blistering of helium-ion-irradiated tungsten," Scr. Mater. **178**, 256–260 (2020).
[24] T. Mewes *et al.*, "Suppression of exchange bias by ion irradiation," Appl. Phys. Lett. **76**(8), 1057–1059 (2000).
[25] M. Nord *et al.*, "Strain anisotropy and magnetic domains in embedded nanomagnets," Small **15**(52), 1904738 (2019).
[26] K. Fallon *et al.*, "Controlled individual skyrmion nucleation at artificial defects formed by ion irradiation," Small **16**(13), 1907450 (2020).
[27] R. Juge *et al.*, "Helium ions put magnetic skyrmions on the track," Nano Lett. **21**(7), 2989–2996 (2021).
[28] S. Ikeda *et al.*, "A perpendicular-anisotropy CoFeB–MgO magnetic tunnel junction," Nat. Mater. **9**(9), 721–724 (2010).
[29] J. Hayakawa *et al.*, "Current-driven magnetization switching in CoFeB/MgO/CoFeB magnetic tunnel junctions," Jpn. J. Appl. Phys. **44**(9L), L1267 (2005).
[30] Y.-T. Chen and S. Xie, "Magnetic and electric properties of amorphous $Co_{40}Fe_{40}B_{20}$ thin films," J. Nanomater. **2012**, 486284.
[31] J. Fassbender, D. Ravelosona, and Y. Samson, "Tailoring magnetism by light-ion irradiation," J. Phys. D: Appl. Phys. **37**(16), R179 (2004).
[32] K. Di *et al.*, "Direct observation of the Dzyaloshinskii–Moriya interaction in a Pt/Co/Ni film," Phys. Rev. Lett. **114**(4), 047201 (2015).
[33] M. Belmeguenai *et al.*, "Brillouin light scattering investigation of the thickness dependence of Dzyaloshinskii–Moriya interaction in $Co_{0.5}Fe_{0.5}$ ultrathin films," Phys. Rev. B **93**(17), 174407 (2016).
[34] X. Chen *et al.*, "Unveiling the emergent traits of chiral spin textures in magnetic multilayers," Adv. Sci. **9**, 2103978 (2022).
[35] G. V. Swamy *et al.*, "Effect of thermal annealing on boron diffusion, microstructural, electrical and magnetic properties of laser ablated CoFeB thin films," AIP Adv. **3**(7), 072129 (2013).
[36] L. Herrera Diez *et al.*, "Controlling magnetic domain wall motion in the creep regime in He^+-irradiated CoFeB/MgO films with perpendicular anisotropy," Appl. Phys. Lett. **107**(3), 032401 (2015).
[37] H. K. Tan *et al.*, "Intermixing induced anisotropy variations in CoB-based chiral multilayer films," J. Phys. D: Appl. Phys. **54**, 354003 (2021).
[38] T. Grehl, "Improvement in TOF-SIMS instrumentation for analytical application and fundamental research," Inaugural-Dissertation zur Erlangung des Doktorgrades der Naturwissenschaften im Fachbereich Physik der Mathematisch-Naturwissenschaftlichen Fakultät der Westfälischen Wilhelms (Universität Münster, 2003).
[39] J.-F. Ying *et al.*, "Investigating the complex mechanism of B migration in a magnetic-tunnel-junction trilayer structure—A combined study using XPS and TOF-SIMS," J. Phys. D: Appl. Phys. **49**(6), 065004 (2015).
[40] M. Raju *et al.*, "Magnetization dynamics and interface studies in ion-beam sputtered Si/CoFeB(8)/MgO(4)/CoFeB(8)/Ta(5) structures," J. Appl. Phys. **115**(17), 17D127 (2014).
[41] W. G. Wang *et al.*, "*In situ* characterization of rapid crystallization of amorphous CoFeB electrodes in CoFeB/MgO/CoFeB junctions during thermal annealing," Appl. Phys. Lett. **95**(24), 242501 (2009).
[42] A. K. Rumaiz *et al.*, "Effects of annealing on the local structure of Fe and Co in CoFeB/MgO/CoFeB tunnel junctions: An extended x-ray-absorption fine structure study," Appl. Phys. Lett. **96**(11), 112502 (2010).
[43] J. C. Read, P. G. Mather, and R. A. Buhrman, "X-ray photoemission study of CoFeB/MgO thin film bilayers," Appl. Phys. Lett. **90**(13), 132503 (2007).
[44] A. T. Hindmarch *et al.*, "Fe diffusion, oxidation, and reduction at the CoFeB/MgO interface studied by soft x-ray absorption spectroscopy and magnetic circular dichroism," Appl. Phys. Lett. **96**(9), 092501 (2010).
[45] M. J. Bonder *et al.*, "Ion irradiation of Co/Pt multilayer films," J. Appl. Phys. **93**(10), 7226–7228 (2003).
[46] M. Dineva-Stavreva, "Monte-Carlo simulation of ion-beam irradiation to defect production on high-temperature superconductors," in *Hochtemperatursupraleitern* (Univ. Wien Bibliothek, Austria, 2005).
[47] W. J. Weber and Y. Zhang, "Predicting damage production in monoatomic and multi-elemental targets using stopping and range of ions in matter code: Challenges and recommendations," Curr. Opin. Solid State Mater. Sci. **23**(4), 100757 (2019).
[48] H. T. Nembach *et al.*, "Tuning of the Dzyaloshinskii–Moriya interaction by He^+ ion irradiation," J. Appl. Phys. **13**(14), 143901 (2022).
[49] C. L. Platt, N. K. Minor, and T. J. Klemmer, "Magnetic and structural properties of FeCoB thin films," IEEE Trans. Magn. **37**(4), 2302–2304 (2001).
[50] A. Yang *et al.*, "Effects of boron addition to the atomic structure and soft magnetic properties of FeCoB films," J. Appl. Phys. **103**(7), 07E736 (2008).
[51] A. K. C. Tan *et al.*, "Skyrmion generation from irreversible fission of stripes in chiral multilayer films," Phys. Rev. Mater. **4**(11), 114419 (2020).
[52] B. Zimmermann *et al.*, "Dzyaloshinskii–Moriya interaction at disordered interfaces from *ab initio* theory: Robustness against intermixing and tunability through dusting," Appl. Phys. Lett. **113**(23), 232403 (2018).

[53]A. Moskaltsova *et al.*, "Impact of the magnetic proximity effect in Pt on the total magnetic moment of Pt/Co/Ta trilayers studied by x-ray resonant magnetic reflectivity," AIP Adv. **10**(1), 015154 (2020).
[54]C. Klewe *et al.*, "Static magnetic proximity effect in Pt/$Ni_{1-x}Fe_x$ bilayers investigated by x-ray resonant magnetic reflectivity," Phys. Rev. B **93**(21), 214440 (2016).
[55]P. Bougiatioti *et al.*, "Impact of magnetic moment and anisotropy of $Co_{1-x}Fe_x$ thin films on the magnetic proximity effect of Pt," arXiv:1807.09032 (2018).
[56]M. Caminale *et al.*, "Spin pumping damping and magnetic proximity effect in Pd and Pt spin-sink layers," Phys. Rev. B **94**(1), 014414 (2016).
[57]Y.-H. Wang *et al.*, "Interfacial and annealing effects on magnetic properties of CoFeB thin films," J. Appl. Phys. **99**(8), 08M307 (2006).
[58]T. Devolder *et al.*, "Magnetic properties of He^+-irradiated Pt/Co/Pt ultrathin films," Phys. Rev. B **64**(6), 064415 (2001).
[59]M. S. El Hadri *et al.*, "Suppression of all-optical switching in He^+-irradiated Co/Pt multilayers: Influence of the domain-wall energy," J. Phys. D: Appl. Phys. **51**(21), 215004 (2018).
[60]A. Casiraghi *et al.*, "Bloch-to-Néel domain wall transition evinced through morphology of magnetic bubble expansion in Ta/CoFeB/MgO layers," arXiv:1907.03708 (2019).
[61]T. Devolder *et al.*, "Irradiation-induced tailoring of the magnetism of CoFeB/MgO ultrathin films," J. Appl. Phys. **113**(20), 203912 (2013).
[62]C.-Y. Yang *et al.*, "Competing anisotropy-tunneling correlation of the CoFeB/MgO perpendicular magnetic tunnel junction: An electronic approach," Sci. Rep. **5**, 17169 (2015).
[63]J. M. Iwata-Harms *et al.*, "Ultrathin perpendicular magnetic anisotropy CoFeB free layers for highly efficient, high speed writing in spin-transfer-torque magnetic random access memory," Sci. Rep. **9**(1), 19407 (2019).
[64]S. Al Risi *et al.*, "Magnetic domain structure and magnetization reversal in (Co/Ni) and (Co/Pd) multilayers," J. Magn. Magn. Mater. **503**, 166579 (2020).
[65]S. Emori *et al.*, "Current-driven dynamics of chiral ferromagnetic domain walls," Nat. Mater. **12**(7), 611–616 (2013).
[66]S. Woo *et al.*, "Observation of room-temperature magnetic skyrmions and their current-driven dynamics in ultrathin metallic ferromagnets," Nat. Mater. **15**(5), 501–506 (2016).
[67]S. Tacchi *et al.*, "Interfacial Dzyaloshinskii–Moriya interaction in Pt/CoFeB films: Effect of the heavy-metal thickness," Phys. Rev. Lett. **118**(14), 147201 (2017).
[68]L. H. Diez *et al.*, "Enhancement of the Dzyaloshinskii–Moriya interaction and domain wall velocity through interface intermixing in Ta/CoFeB/MgO," Phys. Rev. B **99**(5), 054431 (2019).
[69]A. W. Wells *et al.*, "Effect of interfacial intermixing on the Dzyaloshinskii–Moriya interaction in Pt/Co/Pt," Phys. Rev. B **95**(5), 054428 (2017).
[70]A. Vansteenkiste *et al.*, "The design and verification of MuMax3," AIP Adv. **4**(10), 107133 (2014).
[71]I. Lemesh, F. Buttner, and G. S. D. Beach, "Accurate model of the stripe domain phase of perpendicularly magnetized multilayers," Phys. Rev. B **95**(17), 174423 (2017).
[72]P. Agrawal *et al.*, "Measurement of interfacial Dzyaloshinskii–Moriya interaction from static domain imaging," Phys. Rev. B **100**(10), 104430 (2019).
[73]Y. Nahas *et al.*, "Inverse transition of labyrinthine domain patterns in ferroelectric thin films," Nature **577**(7788), 47–51 (2020).
[74]S.-G. Je *et al.*, "Targeted writing and deleting of magnetic skyrmions in two-terminal nanowire devices," Nano Lett. **21**(3), 1253–1259 (2021).
[75]R. Soucaille *et al.*, "Probing the Dzyaloshinskii–Moriya interaction in CoFeB ultrathin films using domain wall creep and Brillouin light spectroscopy," Phys. Rev. B **94**(10), 104431 (2016).
[76]Y. Yoshimura *et al.*, "Soliton-like magnetic domain wall motion induced by the interfacial Dzyaloshinskii–Moriya interaction," Nat. Phys. **12**(2), 157–161 (2016).
[77]P. Lai *et al.*, "An improved racetrack structure for transporting a skyrmion," Sci. Rep. **7**, 45330 (2017).
[78]S. Bhatti and S. N. Piramanayagam, "Effect of Dzyaloshinskii–Moriya interaction energy confinement on current-driven dynamics of skyrmions," Phys. Status Solidi RRL **13**(11), 1900090 (2019).
[79]M. T. Johnson *et al.*, "Magnetic anisotropy in metallic multilayers," Rep. Prog. Phys. **59**(11), 1409 (1996).
[80]R. C. O'handley, *Modern Magnetic Materials: Principles and Applications* (Wiley, 2000).
[81]J. Lourembam *et al.*, "Thickness-dependent perpendicular magnetic anisotropy and Gilbert damping in Hf/$Co_{20}Fe_{60}B_{20}$/MgO heterostructures," Phys. Rev. Appl. **10**(4), 044057 (2018).
[82]K. Shahbazi *et al.*, "Magnetic properties and field-driven dynamics of chiral domain walls in epitaxial Pt/Co/Au_xPt_{1-x} trilayers," Phys. Rev. B **98**(21), 214413 (2018).
[83]A. K. C. Tan *et al.*, "Visualizing the strongly reshaped skyrmion Hall effect in multilayer wire devices," Nat. Commun. **12**(1), 4252 (2021).